First-Principles Equation of State of Polystyrene and Its Effect on Inertial Confinement Fusion Implosions

Controlled inertial confinement fusion (ICF)[1] has been pursued in laboratories for decades as a possibly viable route to clean energy. Materials involved in ICF target implosions undergo extreme plasma conditions such as warm dense matter (WDM) of temperatures from a few to several hundreds of electron volts and densities from 10^{21} to 10^{25} ions/cm^3. The properties of materials in this critical WDM regime have received much attention because of the wide existence of such extreme conditions in the interiors of giant exoplanets,[2] the atmospheres of stars,[3] and laser-produced plasmas,[4] in addition to ICF capsules. Precisely determining the properties of WDM has proved challenging since the strong coupling and quantum effects play a critical role in these complex systems. High-energy-density (HED) experiments,[5–7] equipped with accurate diagnostic tools such as x-ray Thomson scattering[8–10] and x-ray absorption spectroscopy,[11,12] have begun to provide detailed tests of various theoretical models of WDM.

For ICF capsules consisting of a cryogenic deuterium–tritium (DT) fuel covered by an ablator layer, accurate knowledge of the ablator and DT material properties would advance the understanding of target performance, leading to improved ICF target designs.[13] The microphysics responsible for the static, dynamic, and optical properties of DT and ablators determines not only the shock strength and timing[14,15] but also ionization stages,[16] thermal conduction,[17] and nonuniformity growth[18] in ICF implosions. In particular, the equation of state (EOS) of DT and ablators is essential to closing the hydrodynamic equations for ICF simulations and determining the material compressibility[19] and mass ablation rate,[20] which, in turn, control the implosion velocity and the growth of the Rayleigh–Taylor instability.[18] In addition, an accurate EOS of ablators can lead to better predictions of the blowoff plasma con ditions, which helps tighten the laser–plasma interaction models used in integrated ICF simulations. Precisely determining the EOS of materials under HED conditions has remained elusive in the past because of the complexity that different interactions need to be fully taken into account. A variety of physics models have been adopted to compute the EOS of materials. For example, the *SESAME* EOS library[21] was based on the chemical model of matter, while the quotidian equation of state (QEOS)[22] was derived from the improved Thomas–Fermi model. The *SESAME* model used a Helmholtz free energy consisting of a cold curve, an ion thermal contribution, and thermal excitation of electrons calculated by the Thomas–Fermi–Dirac average-atom model. Although such global EOS models have been useful and widely used in the past, their accuracy is worth re-examining in order to make reliable ICF designs and to constrain a laser–plasma interaction model since the margin for ignition is typically small.

Hydrocarbon polymers, such as polystyrene (CH), are often chosen as ablators in both indirect-drive[23–25] and direct-drive[26–28] ICF targets because they are inexpensive and easy to make. Upon laser or x-ray irradiation, CH can be shocked to high pressures from Mbar to Gbar. Depending on the driving laser or x-ray pulse shape, the shocked CH may also relax to a temperature well below ~5 eV at near-solid densities. Just as important as the properties of the DT fuel[29–45] are to ICF implosions, accurate knowledge of the CH ablator in the WDM regime is also crucial for reliable ICF designs. Studies of plasma properties under HED conditions have become possible in recent years because of advances in first-principles methods. These first-principles investigations have covered the static EOS of a variety of materials including hydrogen/deuterium,[29–45] carbon,[46] polystyrene,[47–50] and polyethylene,[51] as well as the transport and optical properties of hydrogen/deuterium[17,52–57] in the WDM regime.

In contrast to previous EOS studies of CH in limited ranges of densities and temperatures, we have combined two first-principles methods—the Kohn–Sham density-functional-theory–based molecular dynamics (KSMD) method[58,59] and the orbital-free molecular dynamics (OFMD) method[60]—to investigate the global EOS of CH in a wide range of plasma conditions. The KSMD method was implemented in the Vienna *ab initio* simulation package (VASP)[61–63] using the Perdew–Burke–Ernzerhof (PBE) exchange-correlation func-

tion.[64] Both KSMD and OFMD methods take the many-body coupling and electron degeneracy effects fully into account. The KSMD calculations cover the low-temperature conditions up to the Fermi temperature (T_F), while the OFMD method is used for higher temperatures. In this article, we report on the first-principles EOS (FPEOS) table of CH and its comparisons with both experiments and the *SESAME* model that is currently used in our hydrocodes.[65] In particular, we illustrate the importance of an accurate CH ablator EOS to understand the one-dimensional (1-D) physics of ICF implosions through radiation–hydrodynamic simulations.

The FPEOS table of CH has been constructed from the KSMD–OFMD calculations for a wide range of densities $\rho = 0.1$ to 100 g/cm^3 and temperatures $T = 1{,}000$ to 4,000,000 K. The KSMD calculations cover all densities except $\rho = 0.1$ g/cm^3 for plasma temperatures up to T_F, while the OFMD method computes higher-temperature and lower-density conditions. These FPEOS data fully cover the plasma conditions of an ablating CH shell. A supercell containing 250 to 432 atoms (C:H = 1:1) with periodic boundary conditions was used. To make the KSMD–OFMD results into a global EOS table for wide HED applications, we also used OFMD calculations to guide the linear extrapolation of the FPEOS data to both low-density and high-temperature points outside the direct calculations. The global FPEOS table of CH was implemented into the hydrocode *LILAC*[65] for ICF implosion simulations.

The FPEOS of CH is first compared with experiments and the *SESAME* EOS model. Figure 143.1 (solid lines) plots the principal Hugoniot predicted by our KSMD–OFMD calculations. The KSMD predictions are made to ~60 Mbar, while the OFMD calculations take over and extend up to the high pressure of $P \simeq 5$ Gbar. The Hugoniot matching at around $P \sim 20$ to 30 Mbar from the two first-principles (FP) calculations was performed with the "boot-strapping" technique.[66] This technique uses the Hugoniot matching to infer the internal energy E_0 of initial solid CH at room temperature for the OFMD dataset. As seen in Fig. 143.1(a), the global Hugoniot predicted from the KSMD–OFMD calculations smoothly extends from a low pressure of ~0.2 Mbar to 5 Gbar. The OFMD matchings at both $T = 120{,}000$ K and $T = 220{,}000$ K give almost identical Hugoniot predictions at high pressures. In comparison with the widely used *SESAME* EOS model (Table 7593),[21] the FP calculations predict CH being slightly stiffer in the pressure range of 5 to 80 Mbar

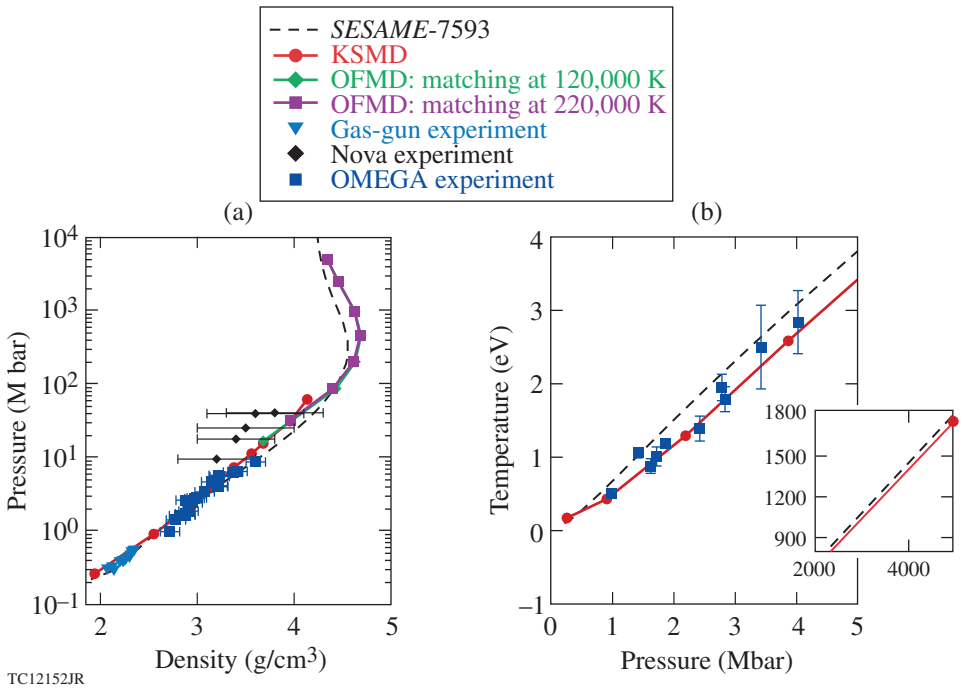

Figure 143.1
(a) The principal Hugoniot pressure as a function of shock density; (b) the temperature of Hugoniot versus pressure. The Kohn–Sham density-functional-theory–based KSMD results (red circles) and the orbital-free molecular-dynamics (OFMD) predictions (purple squares and green diamonds) are compared with the gas-gun experiment,[67] the Nova experiment,[68] and the recent impedance-matching experiment[69] on OMEGA. The prediction of *SESAME*-7593 is plotted with the dashed line.

but softer in higher pressures up to ~5 Gbar. The maximum compression has been shifted from the *SESAME*-predicted ρ_m = 4.55 g/cm^3 at P = 220 Mbar to ρ_m = 4.68 g/cm^3 at P = 440 Mbar in the FPEOS because of the lower temperature inferred from FPEOS [see the inset of Fig. 143.1(b)]. In experiments, the EOS of CH has been extensively studied using gas-gun and laser-driven shock waves. The gas-gun experiment[67] was typically in the low-pressure regime (P < 1 Mbar), while the laser experiments at the Nova[68] and Omega Laser Facilities[69] have recorded shock strengths up to ~40 Mbar. Other shock experiments[49,70,71] of the CH Hugoniot have explored the pressure range of P < 5 Mbar. The available experimental data have been compared with the FPEOS and *SESAME* predictions in Fig. 143.1(a). In the pressure range P < 10 Mbar, both predictions are in good agreement with experiments (within the experimental error). The Hugoniot temperature measured in the recent OMEGA experiment,[69] however, is in much better agreement with the FPEOS prediction [see Fig. 143.1(b)]. The *SESAME* model predicts a maximum of ~30%-higher Hugoniot temperature because it underestimates the internal energy in this pressure range (discussed in detail below). The stiffer behavior of CH, seen in the Nova experiment [e.g., Fig. 143.1(a)] at high pressures of P = 10 to 40 Mbar, seems to qualitatively point toward the FPEOS, even though the experimental error bars were large.

Next, we examine the off-Hugoniot comparison between the FPEOS table and the *SESAME* model in Figs. 143.2 and 143.3, in which the total pressure (P), internal energy (E), and their variations are plotted as functions of CH density for different plasma temperatures. Figures 143.2(a) and 143.2(c) display the direct comparisons of pressure and internal energy between FPEOS (solid lines) and *SESAME* (dashed lines) at T = 15,625 K (≈1.35 eV). At this low temperature, large differences in both P and E appear in the low-density regime of ρ < 3 g/cm^3. To clearly show the variations, the percentage changes of P and E between FPEOS and *SESAME* are plotted in Figs. 143.2(b) and 143.2(d). Figures 143.2(b) and 143.2(d) show that the pressure variations can be as large as approximately –100% in the low-density regime (ρ < 1.0 g/cm^3) and the energy can vary from +40% at ρ = 0.5 g/cm^3 to –20% at high densities. At such a low temperature and not too high densities, it is difficult for models to properly account for all of the important microscopic interactions among the variety of species (atoms, molecules, ions, and electrons) in warm dense plasmas. The first-principles methods take these interactions into account as completely as possible, which can lead to a more-accurate determination of material properties in the WDM regime. When the CH plasma temperature increases to T = 31,250 K (≃2.7 eV) and T = 125,000 K (≃10.8 eV), the many-body and quantum effects become less dominant than in the low-T case. Therefore, the percentage variations between FPEOS and *SESAME*, shown in Fig. 143.3, are reduced as the plasma temperature increases. They change from ±20% at T = 2.7 eV to within ~±10% for the higher temperature of T = 10.8 eV [see Figs. 143.3(b) and 143.3(d)].

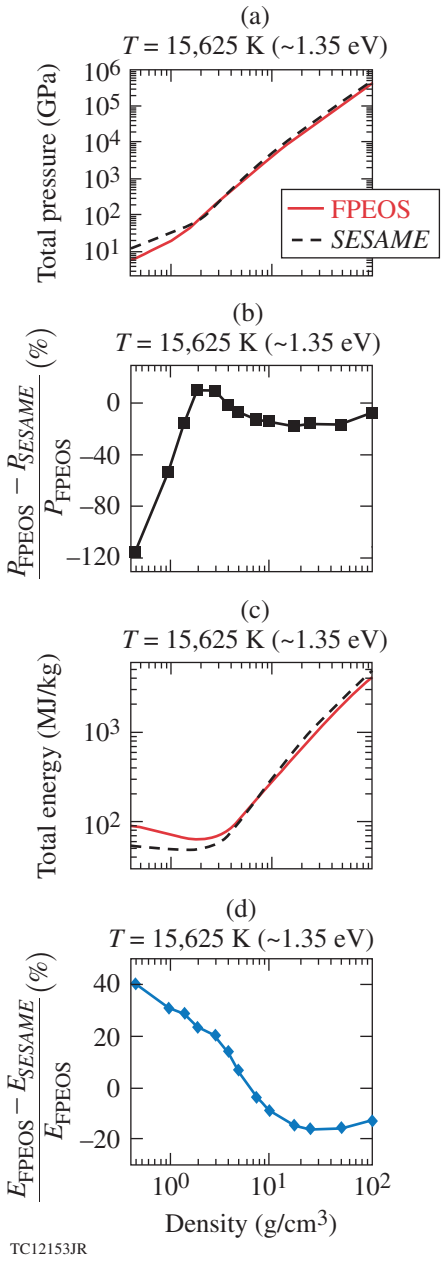

Figure 143.2
The equation-of-state (EOS) comparisons of [(a) and (b)] pressure and [(c) and (d)] internal energy between FPEOS and *SESAME*-7593 as a function of CH density for a plasma temperature of $T \simeq 1.35$ eV. The actual values of pressure and energy are plotted in (a) and (c), while the percentage variations between FPEOS and *SESAME*-7593 are plotted in (b) and (d).

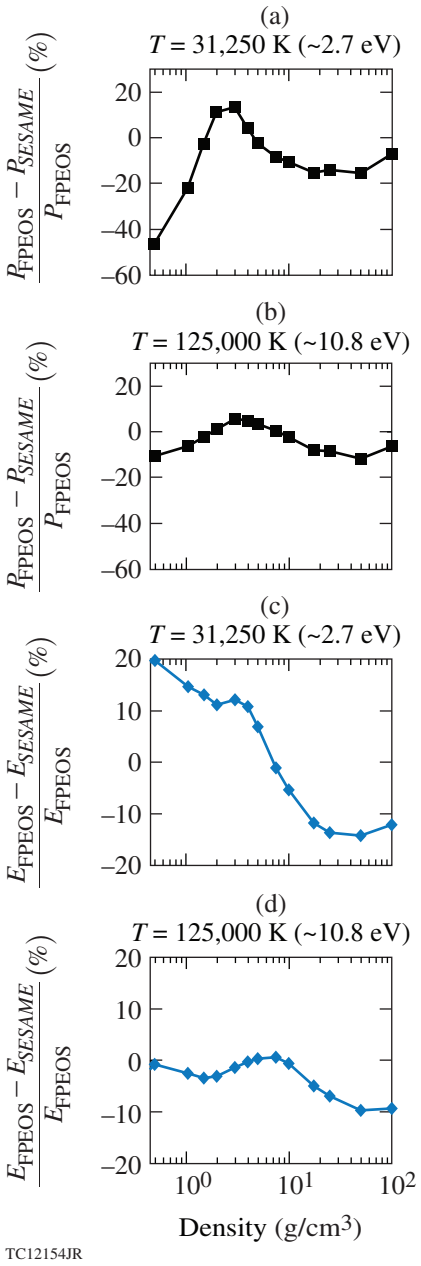

Figure 143.3
Similar to Figs. 143.2(b) and 143.2(d) but for higher plasma temperatures of $T \simeq 2.7$ eV and $T \simeq 10.8$ eV. The variations between FPEOS and *SESAME*-7593 become smaller (toward the ±10% range) as the plasma temperature increases.

With the FPEOS table of CH incorporated into *LILAC*,[65] we can now simulate ICF implosions. By comparing experiments with the hydrodynamic simulations using both FPEOS and *SESAME* models of CH, we can examine how the more-accurate FPEOS of CH affects the 1-D predictions of target performance. As an example, Figs. 143.4 and 143.5 show the two hydro-simulation results for a cryogenic DT target implosion on OMEGA. Figure 143.4(a) plots the triple-picket pulse shape[72–74] with an inset of target dimensions. The cryo-DT target consists of a 49-μm DT layer with an 8.3-μm deuterated plastic (CD) ablator, which is imploded by the low-adiabat laser pulse. The EOS of CD is obtained by mass scaling the FPEOS of CH. The 1-D hydro simulations for both cases have used the same nonlocal thermal-transport model[75] and cross-beam energy transfer model[76,77] in the laser-absorption package. During irradiation of the first laser picket, the plastic is ablated and a shock is launched into the shell. Figure 143.4(b) shows the density and temperature profiles as functions of target radius at $t = 0.5$ ns, in which the FPEOS results (solid lines) are compared to the *SESAME* simulation (dashed lines). At this time, the shock has propagated into the DT layer and the plasma temperature in the CD shell is less than ~5 eV. The relaxation after the shock brings the CD density below the solid level ($\rho_0 = 1.05$ g/cm^3). This is the regime in which large differences (~±20% or more) were found between FPEOS and *SESAME*. As a result, the hydro simulation with FPEOS predicts a lower temperature in the shell (consistent with the lower temperature seen in the shock Hugoniot). This leads to a smaller mass ablation rate of plastic in FPEOS versus *SESAME*, which is shown in Fig. 143.4(c). As the "rocket" effect indicates, less mass ablation rate in FPEOS can lead to a smaller ablation pressure and a slower implosion velocity. We found that at the end of the pulse ($t = 2.5$ ns), the FPEOS-predicted shell travels ~20 μm behind the *SESAME* simulation and the ablation pressure is reduced by ~10%, from 92 Mbar (*SESAME*) to 83 Mbar with FPEOS. Furthermore, the slower ablation can affect the laser light scattering in the coronal plasma. Figure 143.4(d) compares the two predictions with the scattered-light measurement. It shows that the FPEOS simulation gives better agreement with experiment.

Finally, we discuss the overall target performance between the FPEOS and *SESAME* simulations. Figure 143.5(a) plots the implosion velocities and neutron production rates as functions of time. Because of the smaller mass ablation rate of CH predicted by FPEOS [e.g., Fig. 143.4(c)], the implosion velocity is reduced by ~5%, varying from $V_{\text{imp}} \simeq -3.7 \times 10^7$ m/s (*SESAME*) to $V_{\text{imp}} \simeq -3.5 \times 10^7$ m/s (FPEOS). This causes a delay of ~50 ps in the neutron bang time (the time at which the neutron rate reaches peak) for the FPEOS simulation. From the scaling law of $Y \propto V_{\text{imp}}^6$ for the neutron yield,[78–80] the ~5% reduction in V_{imp} can have a significant consequence in neutron production. Figure 143.5(a) shows a lower peak neutron rate in the FPEOS case (blue solid line), which gives a total neutron yield of $Y = 1.1 \times 10^{14}$, dropping from the *SESAME*-predicted value of $Y = 1.5 \times 10^{14}$. At their peak neutron production, Fig. 143.5(b)

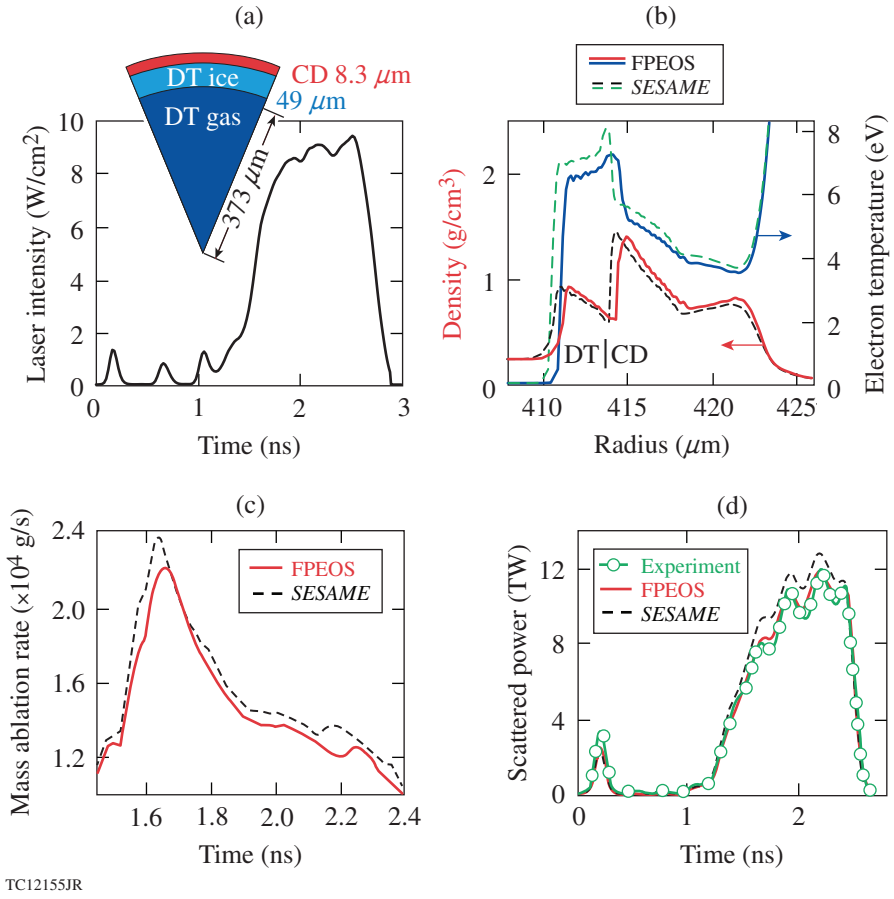

Figure 143.4
The effect of CH-FPEOS on the cryogenic DT target implosion on OMEGA: (a) the triple-picket pulse shape and target dimensions; (b) the density and temperature profiles at $t = 0.5$ ns that are predicted by radiation–hydrodynamic simulations using either FPEOS (solid lines) or *SESAME* (dashed lines) for the plastic ablator; (c) the predicted mass ablation rates as a function of time; and (d) the comparison of scattered-light predictions with experimental measurement.

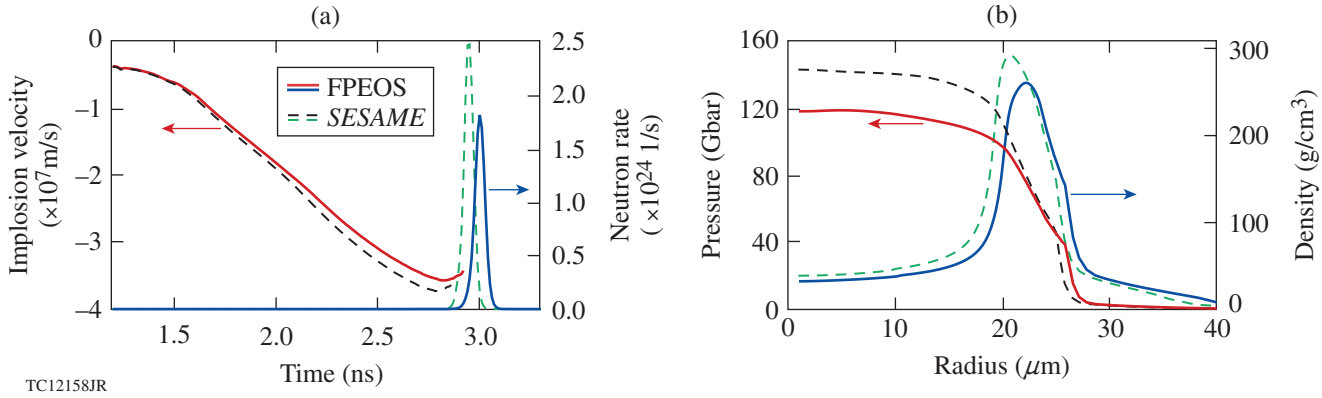

Figure 143.5
Comparisons of the implosion prediction between *SESAME* EOS (dashed lines) and FPEOS (solid lines) of CH: (a) the implosion velocity and neutron-production rate as functions of time and (b) the pressure and density as functions of target radius at peak neutron production.

shows the hot-spot pressure and shell-density degradation in the FPEOS simulation. The hot-spot peak pressure is reduced from P = 142 Gbar (*SESAME*) to P = 118 Gbar (FPEOS), and the DT shell is stagnated at a slightly larger radius and lower peak density for the FPEOS simulation. Also, the neutron-averaged hot-spot temperature decreases from T_i = 3.6 keV (*SESAME*) to T_i = 3.4 keV (FPEOS), although the change in neutron-averaged $\langle \rho R \rangle$ is only moderate (<5%), $\langle \rho R \rangle$ = 262 mg/cm^2 (*SESAME*) versus $\langle \rho R \rangle$ = 250 mg/cm^2 (FPEOS).

In summary, we combined the two *ab initio* methods of KSMD and OFMD to calculate the equation of state for the ICF ablator material of CH, in a wide range of plasma conditions. The Hugoniot's pressure and temperature, predicted from the FPEOS table, are both in better agreement with experiments. Large differences in both pressure and energy have been observed in the low-temperature WDM regime when the FPEOS is compared with the widely used *SESAME* model. Hydro simulations of an ICF target implosion using the FPEOS of CH predict ~5%-lower implosion velocity, ~10% decrease in ablation pressure, and ~30% neutron yield reduction relative to the usual *SESAME* simulation. These are caused by the smaller mass ablation rate predicted by the CH FPEOS. The reduction of ablation velocity may have implications in nonuniformity growth at the ablation front, which will be examined in future multidimensional hydro simulations. Overall, the predicted scattered light with the FPEOS simulation is in better agreement with experimental measurements. Using our more-accurate FPEOS of ablators in hydrodynamic simulations will lead to improved ICF target design and better predictions of HED physics experiments.

ACKNOWLEDGMENT

This material is based upon work supported by the Department of Energy National Nuclear Security Administration under Award Number DE-NA0001944, the University of Rochester, and the New York State Energy Research and Development Authority. The support of DOE does not constitute an endorsement by DOE of the views expressed in this article. This work was also supported by Scientific Campaign 10 at the Los Alamos National Laboratory, operated by Los Alamos National Security, LLC for the National Nuclear Security Administration of the U.S. Department of Energy under Contract No. DE-AC52-06NA25396.

REFERENCES

1. J. Nuckolls *et al*., Nature **239**, 139 (1972).
2. N. C. Santos, W. Benz, and M. Mayor, Science **310**, 251 (2005).
3. G. Fontaine, P. Brassard, and P. Bergeron, Publ. Astron. Soc. Pac. **113**, 409 (2001).
4. B. A. Hammel *et al*., High Energy Density Phys. **6**, 171 (2010); D. H. Froula, D. T. Michel, I. V. Igumenshchev, S. X. Hu, B. Yaakobi, J. F. Myatt, D. H. Edgell, R. Follett, V. Yu. Glebov, V. N. Goncharov, T. J. Kessler, A. V. Maximov, P. B. Radha, T. C. Sangster, W. Seka, R. W. Short, A. A. Solodov, C. Sorce, and C. Stoeckl, Plasma Phys. Control. Fusion **54**, 124016 (2012).
5. S. H. Glenzer and R. Redmer, Rev. Mod. Phys. **81**, 1625 (2009).
6. S. H. Glenzer *et al*., Science **327**, 1228 (2010).
7. A. L. Kritcher *et al*., Phys. Rev. Lett. **107**, 015002 (2011).
8. S. H. Glenzer *et al*., Phys. Rev. Lett. **90**, 175002 (2003).
9. B. Barbrel *et al*., Phys. Rev. Lett. **102**, 165004 (2009).
10. S. P. Regan, K. Falk, G. Gregori, P. B. Radha, S. X. Hu, T. R. Boehly, B. J. B. Crowley, S. H. Glenzer, O. L. Landen, D. O. Gericke, T. Döppner, D. D. Meyerhofer, C. D. Murphy, T. C. Sangster, and J. Vorberger, Phys. Rev. Lett. **109**, 265003 (2012).
11. S. M. Vinko *et al*., Nature **482**, 59 (2012).
12. O. Ciricosta *et al*., Phys. Rev. Lett. **109**, 065002 (2012).
13. S. X. Hu, V. N. Goncharov, T. R. Boehly, R. L. McCrory, S. Skupsky, L. A. Collins, J. D. Kress, and B. Militzer, Phys. Plasmas **22**, 056304 (2015).
14. T. R. Boehly, V. N. Goncharov, W. Seka, M. A. Barrios, P. M. Celliers, D. G. Hicks, G. W. Collins, S. X. Hu, J. A. Marozas, and D. D. Meyerhofer, Phys. Rev. Lett. **106**, 195005 (2011).
15. H. F. Robey *et al*., Phys. Rev. Lett. **111**, 065003 (2013).
16. L. B. Fletcher *et al*., Phys. Rev. Lett. **112**, 145004 (2014).
17. V. Recoules *et al*., Phys. Rev. Lett. **102**, 075002 (2009).
18. V. A. Smalyuk *et al*., Phys. Rev. Lett. **112**, 185003 (2014); V. A. Smalyuk, S. X. Hu, J. D. Hager, J. A. Delettrez, D. D. Meyerhofer, T. C. Sangster, and D. Shvarts, Phys. Rev. Lett. **103**, 105001 (2009).
19. S. X. Hu, V. A. Smalyuk, V. N. Goncharov, J. P. Knauer, P. B. Radha, I. V. Igumenshchev, J. A. Marozas, C. Stoeckl, B. Yaakobi, D. Shvarts, T. C. Sangster, P. W. McKenty, D. D. Meyerhofer, S. Skupsky, and R. L. McCrory, Phys. Rev. Lett. **100**, 185003 (2008).
20. D. T. Michel, A. K. Davis, V. N. Goncharov, T. C. Sangster, S. X. Hu, I. V. Igumenshchev, D. D. Meyerhofer, W. Seka, and D. H. Froula, Phys. Rev. Lett. **114**, 155002 (2015).
21. B. I. Bennett *et al*., Los Alamos National Laboratory, Los Alamos, NM, Report LA-7130 (1978).
22. R. M. More *et al*., Phys. Fluids **31**, 3059 (1988).
23. S. W. Haan, J. D. Lindl, D. A. Callahan, D. S. Clark, J. D. Salmonson, B. A. Hammel, L. J. Atherton, R. C. Cook, M. J. Edwards, S. Glenzer, A. V. Hamza, S. P. Hatchett, M. C. Herrmann, D. E. Hinkel, D. D. Ho, H. Huang, O. S. Jones, J. Kline, G. Kyrala, O. L. Landen, B. J.

MacGowan, M. M. Marinak, D. D. Meyerhofer, J. L. Milovich, K. A. Moreno, E. I. Moses, D. H. Munro, A. Nikroo, R. E. Olson, K. Peterson, S. M. Pollaine, J. E. Ralph, H. F. Robey, B. K. Spears, P. T. Springer, L. J. Suter, C. A. Thomas, R. P. Town, R. Vesey, S. V. Weber, H. L. Wilkens, and D. C. Wilson, Phys. Plasmas **18**, 051001 (2011).

24. M. J. Edwards, J. D. Lindl, B. K. Spears, S. V. Weber, L. J. Atherton, D. L. Bleuel, D. K. Bradley, D. A. Callahan, C. J. Cerjan, D. Clark, G. W. Collins, J. E. Fair, R. J. Fortner, S. H. Glenzer, S. W. Haan, B. A. Hammel, A. V. Hamza, S. P. Hatchett, N. Izumi, B. Jacoby, O. S. Jones, J. A. Koch, B. J. Kozioziemski, O. L. Landen, R. Lerche, B. J. MacGowan, A. J. MacKinnon, E. R. Mapoles, M. M. Marinak, M. Moran, E. I. Moses, D. H. Munro, D. H. Schneider, S. M. Sepke, D. A. Shaughnessy, P. T. Springer, R. Tommasini, L. Bernstein, W. Stoeffl, R. Betti, T. R. Boehly, T. C. Sangster, V. Yu. Glebov, P. W. McKenty, S. P. Regan, D. H. Edgell, J. P. Knauer, C. Stoeckl, D. R. Harding, S. Batha, G. Grim, H. W. Herrmann, G. Kyrala, M. Wilke, D. C. Wilson, J. Frenje, R. Petrasso, K. Moreno, H. Huang, K. C. Chen, E. Giraldez, J. D. Kilkenny, M. Mauldin, N. Hein, M. Hoppe, A. Nikroo, and R. J. Leeper, Phys. Plasmas **18**, 051003 (2011).

25. C. Cherfils-Clérouin *et al*., J. Phys.: Conf. Ser. **244**, 022009 (2010).

26. D. D. Meyerhofer, R. L. McCrory, R. Betti, T. R. Boehly, D. T. Casey, T. J. B. Collins, R. S. Craxton, J. A. Delettrez, D. H. Edgell, R. Epstein, K. A. Fletcher, J. A. Frenje, V. Yu. Glebov, V. N. Goncharov, D. R. Harding, S. X. Hu, I. V. Igumenshchev, J. P. Knauer, C. K. Li, J. A. Marozas, F. J. Marshall, P. W. McKenty, P. M. Nilson, S. P. Padalino, R. D. Petrasso, P. B. Radha, S. P. Regan, T. C. Sangster, F. H. Séguin, W. Seka, R. W. Short, D. Shvarts, S. Skupsky, J. M. Soures, C. Stoeckl, W. Theobald, and B. Yaakobi, Nucl. Fusion **51**, 053010 (2011).

27. R. L. McCrory, R. Betti, T. R. Boehly, D. T. Casey, T. J. B. Collins, R. S. Craxton, J. A. Delettrez, D. H. Edgell, R. Epstein, J. A. Frenje, D. H. Froula, M. Gatu-Johnson, V. Yu. Glebov, V. N. Goncharov, D. R. Harding, M. Hohenberger, S. X. Hu, I. V. Igumenshchev, T. J. Kessler, J. P. Knauer, C. K. Li, J. A. Marozas, F. J. Marshall, P. W. McKenty, D. D. Meyerhofer, D. T. Michel, J. F. Myatt, P. M. Nilson, S. J. Padalino, R. D. Petrasso, P. B. Radha, S. P. Regan, T. C. Sangster, F. H. Séguin, W. Seka, R. W. Short, A. Shvydky, S. Skupsky, J. M. Soures, C. Stoeckl, W. Theobald, B. Yaakobi, and J. D. Zuegel, Nucl. Fusion **53**, 113021 (2013).

28. R. S. Craxton, K. S. Anderson, T. R. Boehly, V. N. Goncharov, D. R. Harding, J. P. Knauer, R. L. McCrory, P. W. McKenty, D. D. Meyerhofer, J. F. Myatt, A. J. Schmitt, J. D. Sethian, R. W. Short, S. Skupsky, W. Theobald, W. L. Kruer, K. Tanaka, R. Betti, T. J. B. Collins, J. A. Delettrez, S. X. Hu, J. A. Marozas, A. V. Maximov, D. T. Michel, P. B. Radha, S. P. Regan, T. C. Sangster, W. Seka, A. A. Solodov, J. M. Soures, C. Stoeckl, and J. D. Zuegel, "Direct-Drive Inertial Confinement Fusion: A Review," to be published in Physics of Plasmas.

29. L. Caillabet, S. Mazevet, and P. Loubeyre, Phys. Rev. B **83**, 094101 (2011).

30. L. Caillabet *et al*., Phys. Rev. Lett. **107**, 115004 (2011).

31. P. Loubeyre, S. Brygoo, J. Eggert, P. M. Celliers, D. K. Spaulding, J. R. Rygg, T. R. Boehly, G. W. Collins, and R. Jeanloz, Phys. Rev. B **86**, 144115 (2012).

32. S. X. Hu, B. Militzer, V. N. Goncharov, and S. Skupsky, Phys. Rev. Lett. **104**, 235003 (2010).

33. S. X. Hu, B. Militzer, V. N. Goncharov, and S. Skupsky, Phys. Rev. B **84**, 224109 (2011).

34. M. A. Morales *et al*., High Energy Density Phys. **8**, 5 (2012).

35. J. Vorberger, D. O. Gericke, and W. D. Kraeft, High Energy Density Phys. **9**, 448 (2013).

36. V. V. Karasiev *et al*., Phys. Rev. B **88**, 161108(R) (2013).

37. C. Pierleoni *et al*., Phys. Rev. Lett. **73**, 2145 (1994).

38. B. Militzer and D. M. Ceperley, Phys. Rev. Lett. **85**, 1890 (2000).

39. J. Clérouin and J.-F. Dufrêche, Phys. Rev. E **64**, 066406 (2001).

40. L. A. Collins *et al*., Phys. Rev. B **63**, 184110 (2001).

41. M. P. Desjarlais, Phys. Rev. B **68**, 064204 (2003).

42. B. Holst, R. Redmer, and M. P. Desjarlais, Phys. Rev. B **77**, 184201 (2008).

43. C. Wang and P. Zhang, Phys. Plasmas **20**, 092703 (2013).

44. A. Becker *et al*., Astrophys. J. Suppl. Ser. **215**, 21 (2014).

45. L. X. Benedict, "A Review of Equation of State Models for Hydrogen," to be published in *World Scientific Review*.

46. R. F. Smith *et al*., Nature **511**, 330 (2014).

47. C. Wang, X.-T. He, and P. Zhang, Phys. Plasmas **18**, 082707 (2011).

48. F. Lambert and V. Recoules, Phys. Rev. E **86**, 026405 (2012).

49. S. Hamel, L. X. Benedict, P. M. Celliers, M. A. Barrios, T. R. Boehly, G. W. Collins, T. Döppner, J. H. Eggert, D. R. Farley, D. G. Hicks, J. L. Kline, A. Lazicki, S. LePape, A. J. Mackinnon, J. D. Moody, H. F. Robey, E. Schwegler, and P. A. Sterne, Phys. Rev. B **86**, 094113 (2012).

50. S. X. Hu, T. R. Boehly, and L. A. Collins, Phys. Rev. E **89**, 063104 (2014).

51. T. R. Mattsson *et al*., Phys. Rev. B **81**, 054103 (2010).

52. B. Holst, M. French, and R. Redmer, Phys. Rev. B **83**, 235120 (2011).

53. F. Lambert *et al*., Phys. Plasmas **18**, 056306 (2011).

54. C. E. Starrett *et al*., Phys. Plasmas **19**, 102709 (2012).

55. S. X. Hu, L. A. Collins, T. R. Boehly, J. D. Kress, V. N. Goncharov, and S. Skupsky, Phys. Rev. E **89**, 043105 (2014).

56. S. X. Hu, L. A. Collins, V. N. Goncharov, T. R. Boehly, R. Epstein, R. L. McCrory, and S. Skupsky, Phys. Rev. E **90**, 033111 (2014).

57 G. Faussurier and C. Blancard, Phys. Plasmas **22**, 042701 (2015).

58. L. Collins *et al*., Phys. Rev. E **52**, 6202 (1995).

59. J. G. Clérouin and S. Bernard, Phys. Rev. E **56**, 3534 (1997).

60. F. Lambert, J. Clérouin, and G. Zérah, Phys. Rev. E **73**, 016403 (2006).

61. G. Kresse and J. Hafner, Phys. Rev. B **47**, 558 (1993).

62. G. Kresse and J. Hafner, Phys. Rev. B **49**, 14,251 (1994).

63. G. Kresse and J. Furthmüller, Phys. Rev. B **54**, 11169 (1996).

64. J. P. Perdew, K. Burke, and M. Ernzerhof, Phys. Rev. Lett. **77**, 3865 (1996); *ibid*. **78**, 1396(E) (1997).

65. J. Delettrez, R. Epstein, M. C. Richardson, P. A. Jaanimagi, and B. L. Henke, Phys. Rev. A **36**, 3926 (1987).

66. D. Sheppard *et al*., Phys. Rev. E **90**, 063314 (2014).

67. S. P. Marsh, ed. *LASL Shock Hugoniot Data*, Los Alamos Series on Dynamic Material Properties (University of California Press, Berkeley, CA, 1980).

68. R. Cauble *et al*., Phys. Plasmas **4**, 1857 (1997).

69. M. A. Barrios, D. G. Hicks, T. R. Boehly, D. E. Fratanduono, J. H. Eggert, P. M. Celliers, G. W. Collins, and D. D. Meyerhofer, Phys. Plasmas **17**, 056307 (2010).

70. M. Koenig *et al*., Phys. Plasmas **10**, 3026 (2003).

71. N. Ozaki *et al*., Phys. Plasmas **16**, 062702 (2009).

72. V. N. Goncharov, T. C. Sangster, T. R. Boehly, S. X. Hu, I. V. Igumenshchev, F. J. Marshall, R. L. McCrory, D. D. Meyerhofer, P. B. Radha, W. Seka, S. Skupsky, C. Stoeckl, D. T. Casey, J. A. Frenje, and R. D. Petrasso, Phys. Rev. Lett. **104**, 165001 (2010).

73. T. C. Sangster, V. N. Goncharov, R. Betti, P. B. Radha, T. R. Boehly, D. T. Casey, T. J. B. Collins, R. S. Craxton, J. A. Delettrez, D. H. Edgell, R. Epstein, C. J. Forrest, J. A. Frenje, D. H. Froula, M. Gatu-Johnson, V. Yu. Glebov, D. R. Harding, M. Hohenberger, S. X. Hu, I. V. Igumenshchev, R. Janezic, J. H. Kelly, T. J. Kessler, C. Kingsley, T. Z. Kosc, J. P. Knauer, S. J. Loucks, J. A. Marozas, F. J. Marshall, A. V. Maximov, R. L. McCrory, P. W. McKenty, D. D. Meyerhofer, D. T. Michel, J. F. Myatt, R. D. Petrasso, S. P. Regan, W. Seka, W. T. Shmayda, R. W. Short, A. Shvydky, S. Skupsky, J. M. Soures, C. Stoeckl, W. Theobald, V. Versteeg, B. Yaakobi, and J. D. Zuegel, Phys. Plasmas **20**, 056317 (2013).

74. S. X. Hu, V. N. Goncharov, P. B. Radha, J. A. Marozas, S. Skupsky, T. R. Boehly, T. C. Sangster, D. D. Meyerhofer, and R. L. McCrory, Phys. Plasmas **17**, 102706 (2010).

75. V. N. Goncharov, T. C. Sangster, P. B. Radha, R. Betti, T. R. Boehly, T. J. B. Collins, R. S. Craxton, J. A. Delettrez, R. Epstein, V. Yu. Glebov, S. X. Hu, I. V. Igumenshchev, J. P. Knauer, S. J. Loucks, J. A. Marozas, F. J. Marshall, R. L. McCrory, P. W. McKenty, D. D. Meyerhofer, S. P. Regan, W. Seka, S. Skupsky, V. A. Smalyuk, J. M. Soures, C. Stoeckl, D. Shvarts, J. A. Frenje, R. D. Petrasso, C. K. Li, F. Séguin, W. Manheimer, and D. G. Colombant, Phys. Plasmas **15**, 056310 (2008).

76. I. V. Igumenshchev, W. Seka, D. H. Edgell, D. T. Michel, D. H. Froula, V. N. Goncharov, R. S. Craxton, L. Divol, R. Epstein, R. Follett, J. H. Kelly, T. Z. Kosc, A. V. Maximov, R. L. McCrory, D. D. Meyerhofer, P. Michel, J. F. Myatt, T. C. Sangster, A. Shvydky, S. Skupsky, and C. Stoeckl, Phys. Plasmas **19**, 056314 (2012); D. H. Froula, T. J. Kessler, I. V. Igumenshchev, R. Betti, V. N. Goncharov, H. Huang, S. X. Hu, E. Hill, J. H. Kelly, D. D. Meyerhofer, A. Shvydky, and J. D. Zuegel, Phys. Plasmas **20**, 082704 (2013).

77. V. N. Goncharov, T. C. Sangster, R. Betti, T. R. Boehly, M. J. Bonino, T. J. B. Collins, R. S. Craxton, J. A. Delettrez, D. H. Edgell, R. Epstein, R. K. Follet, C. J. Forrest, D. H. Froula, V. Yu. Glebov, D. R. Harding, R. J. Henchen, S. X. Hu, I. V. Igumenshchev, R. Janezic, J. H. Kelly, T. J. Kessler, T. Z. Kosc, S. J. Loucks, J. A. Marozas, F. J. Marshall, A. V. Maximov, R. L. McCrory, P. W. McKenty, D. D. Meyerhofer, D. T. Michel, J. F. Myatt, R. Nora, P. B. Radha, S. P. Regan, W. Seka, W. T. Shmayda, R. W. Short, A. Shvydky, S. Skupsky, C. Stoeckl, B. Yaakobi, J. A. Frenje, M. Gatu-Johnson, R. D. Petrasso, and D. T. Casey, Phys. Plasmas **21**, 056315 (2014).

78. M. C. Herrmann, M. Tabak, and J. D. Lindl, Nucl. Fusion **41**, 99 (2001).

79. C. D. Zhou and R. Betti, Phys. Plasmas **15**, 102707 (2008)

80. R. Nora, R. Betti, K. S. Anderson, A. Shvydky, A. Bose, K. M. Woo, A. R. Christopherson, J. A. Marozas, T. J. B. Collins, P. B. Radha, S. X. Hu, R. Epstein, F. J. Marshall, R. L. McCrory, T. C. Sangster, and D. D. Meyerhofer, Phys. Plasmas **21**, 056316 (2014).